

Supporting Information

Carbon-wrapped vanadium dioxide for aqueous zinc batteries based on in-situ carbon-impregnation engineering

Xianyu Liu^{a,*}, Lei Tao^a, Yande Zhao^a, Hongmei Cao^{*b}, Zhe Wang^c and Zhigang Fan^{*d}

^a Bailie School of Petroleum Engineering, Lanzhou City University, Lanzhou 730070, China.

^b School of Energy and Power, Jiangsu University of Science and Technology, Zhenjiang, Jiangsu, 212003 PR China.

^c School of Automotive Engineering, Jilin Engineering Vocational College, Siping 136000, Jilin, China.

^d National Petroleum and Natural Gas Pipeline Network Group Co., Ltd, Yunnan Branch, Kunming, 650032, China.

Corresponding Author

Xianyu Liu, E-mail: xyliu15@mail.ustc.edu.cn

Hongmei Cao, E-mail: caohm@just.edu.cn

Zhigang Fan, E-mail: fengdediaolin@163.com

Experiment and methods

Synthesis of VO₂@C composites

Typically, 0.45 g of V₂O₅ was added in 36 mL of H₂O₂ (5%), denoted as Solution A. Next, 0.2 g, 0.4 g or 0.6 g of glucose was dissolved in H₂O (10 mL), respectively, which was denoted as solution B. Then, the solution B was slowly added to solution A, and the mixture was stirred for 4 h at room temperature (RT). Afterward, the mixed solution was transferred into a reactor (50 mL) and maintained at 200 °C for 4 h. After cooling to RT, the precipitate was washed using water and ethanol. Finally, the VO₂@C composites were vacuum-dried at 80 °C (24 h). The as-prepared composites with different contents of glucose were designated as VO₂@C1 (0.2 g), VO₂@C2 (0.4 g), and VO₂@C3 (0.6 g), respectively.

Preparation of Zn//VO₂@C Batteries

The VO₂@C composite was mixed with conductive carbon and PVDF binder in N-methyl pyrrolidone (NMP) with a mass ratio of 8:1:1. The electrode preparation process was finished by coating the resulting slurry onto stencils and dried for overnight. The average mass loading of active material was maintained at approximately 1.5 mg cm⁻². The coin-type battery was assembled using the VO₂@C electrode as cathode, filter paper as separator, and zinc foil as anode. Moreover, 3 M Zn(CF₃SO₃)₂ aqueous solution was employed as electrolyte. The dosage of electrolyte is 100 μL for each cell.

Material characterization

The morphologies of prepared VO₂@C composites were characterized by using high-resolution transmission electron microscopy (TEM, JEOL 2100F) and field-emission scanning electron microscopy (SEM, SUPRA 55). X-ray diffraction (XRD) analysis was performed with a Bruker D8 Advance powder diffractometer with Cu

$K\alpha$ radiation. A multifunctional X-ray photoelectron spectroscopy (XPS, Perkin Elmer PHI 1600 ESCA) was employed for examining the valence and surface composition of the $\text{VO}_2@\text{C}$ composites. In order to determine the carbon content in $\text{VO}_2@\text{C}$ composites, thermal gravimetric analysis (TGA, NETZSCH) was conducted between 25 and 600 °C in an air atmosphere.

Electrochemical measurements

Battery test systems (LAND CT2001A) were used to obtain the results for galvanostatic charge/discharge, long-term cycling, and galvanostatic intermittent titration technique (GITT) tests. Cyclic voltammetry (CV) and electrochemical impedance spectroscopy (EIS) studies were carried out employing an electrochemical workstation (CHI660E). CV assessments were conducted across various scan rates ($0.2\text{-}1.0\text{ mV s}^{-1}$) in a potential range (0.3-1.6 V), while EIS measurements spanned frequencies from 10 mHz to 100 KHz. The specific capacities were calculated based on the mass of the $\text{VO}_2@\text{C}$ materials.

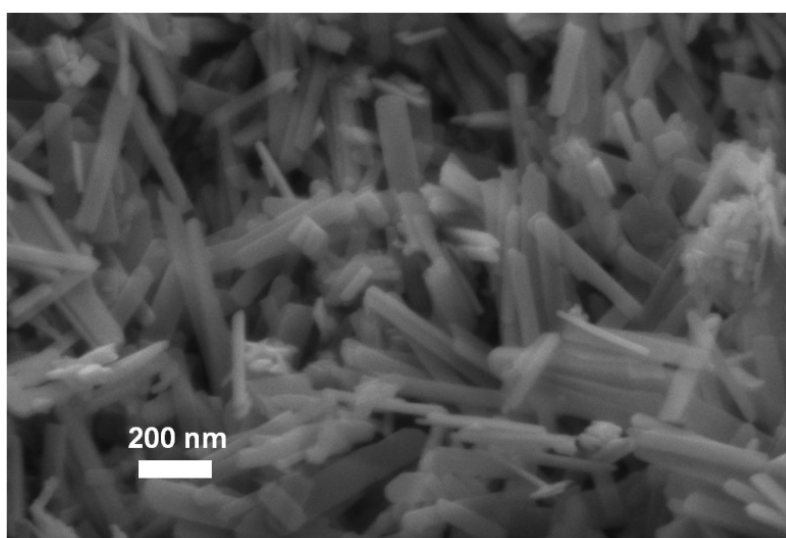


Fig. S1. SEM image of $\text{VO}_2@\text{C}1$.

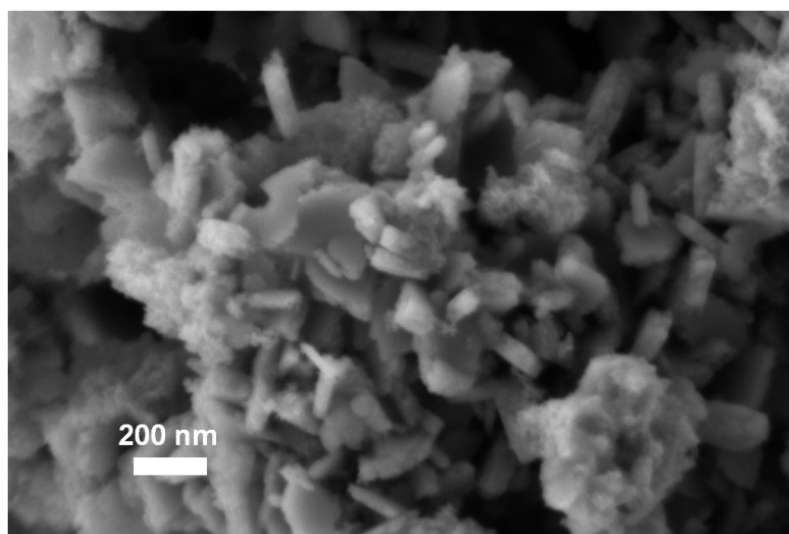


Fig. S2. SEM image of VO₂@C3.

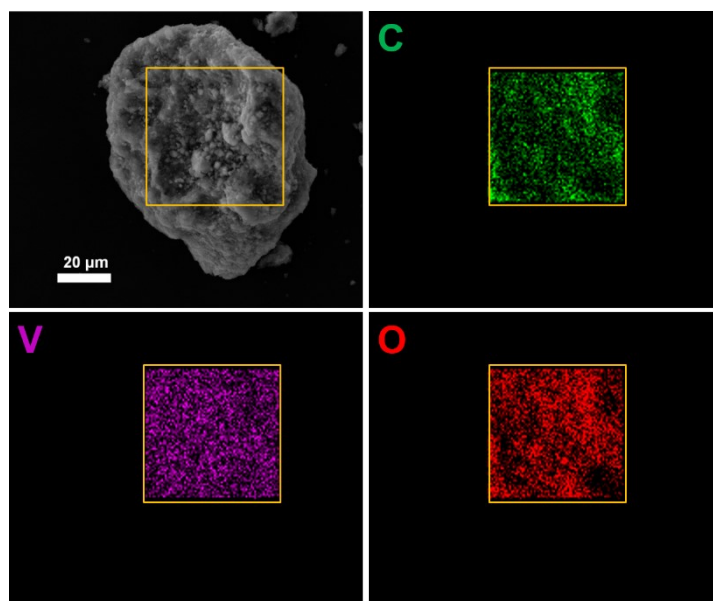


Fig. S3. EDS images of VO₂@C2.

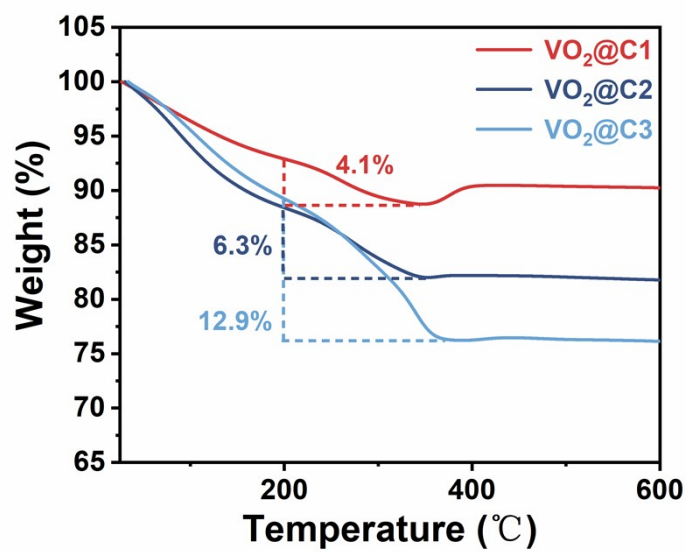


Fig. S4. TG curves of VO₂@C.

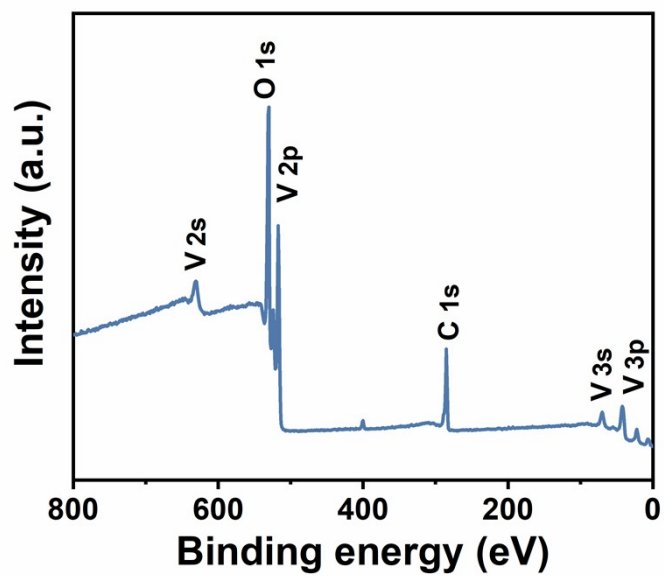


Fig. S5. XPS survey full scan spectrum of the VO₂@C2.

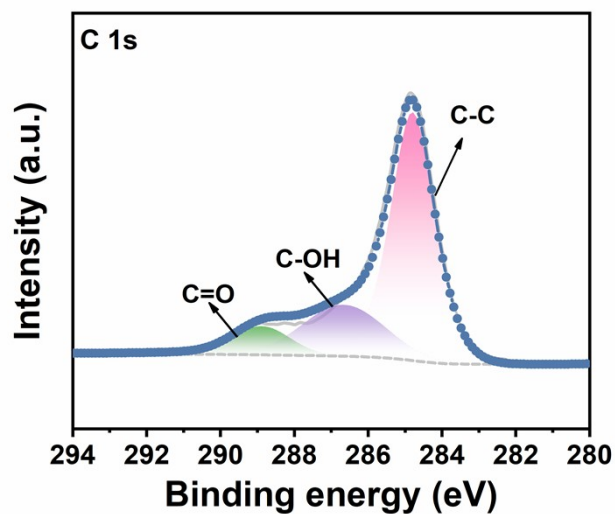


Fig. S6. C1s XPS spectrum of the VO₂@C2.

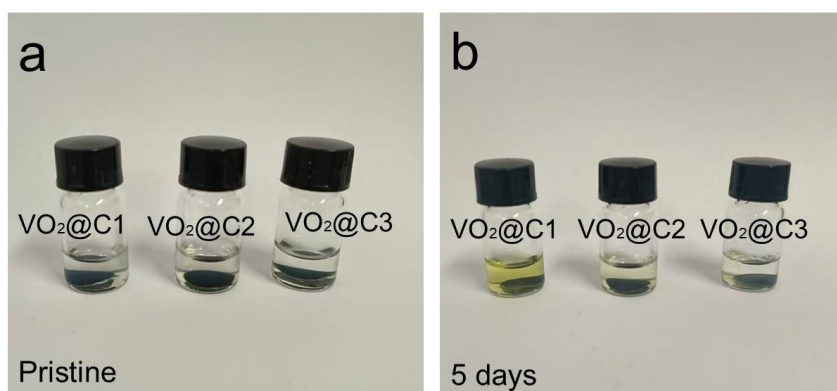


Fig. S7. VO₂@C1, VO₂@C2, and VO₂@C3 electrodes soaked in the electrolyte (a) Pristine and (b) 5 days.

Note to Fig. S7:

After soaked in electrolyte for 5 days, the electrolyte soaked VO₂@C1 electrode turned yellow due to the dissolving of V element. In contrast, the electrolytes soaked VO₂@C2, and VO₂@C3 still kept nearly transparent, which indicated that more carbon content would restrain the dissolution (Fig. S7).

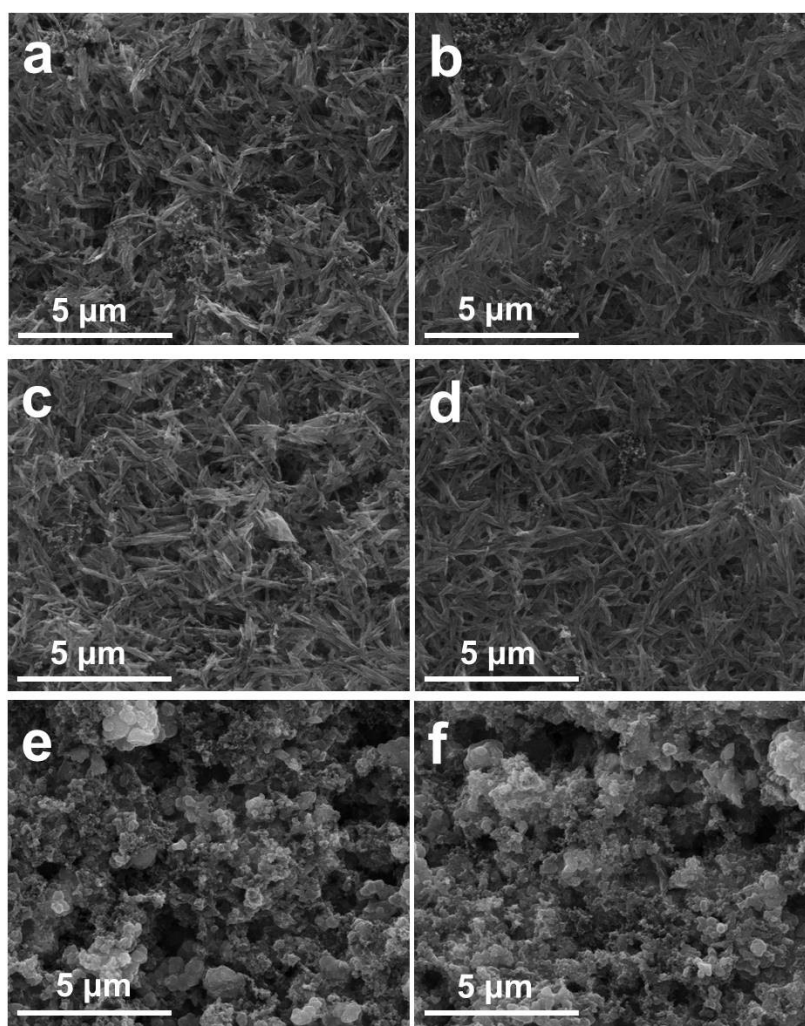


Fig. S8 SEM images of electrodes soaked in the electrolyte (a) Pristine of VO₂@C1; (b) VO₂@C1 for 5 days; (c) Pristine of VO₂@C2; (d) VO₂@C2 for 5 days; (e) Pristine of VO₂@C3 and (f) VO₂@C3 for 5 days.

Note to Fig. S8:

The SEM images show that the morphology of VO₂@C1, VO₂@C2, and VO₂@C3 electrodes has no obvious change (Fig. S8)

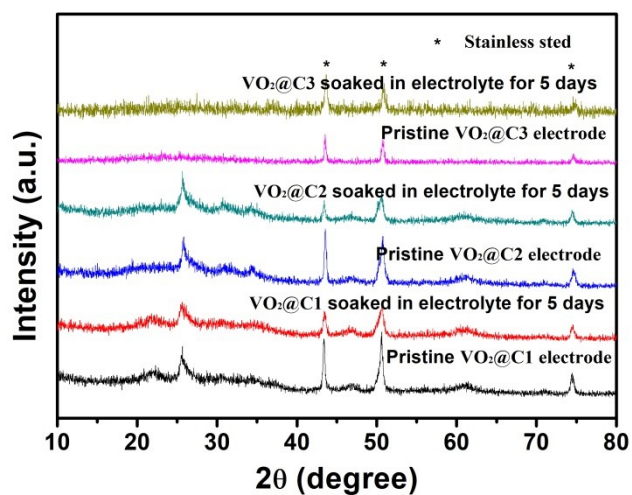


Fig. S9 XRD patterns of electrodes soaked in the electrolyte for 5 days.

Note to Fig. S9:

The XRD patterns of electrodes soaked in the electrolyte for 5 days are similar with that of pristine curves (Fig. S9), which agree with the SEM results (Fig. S7).

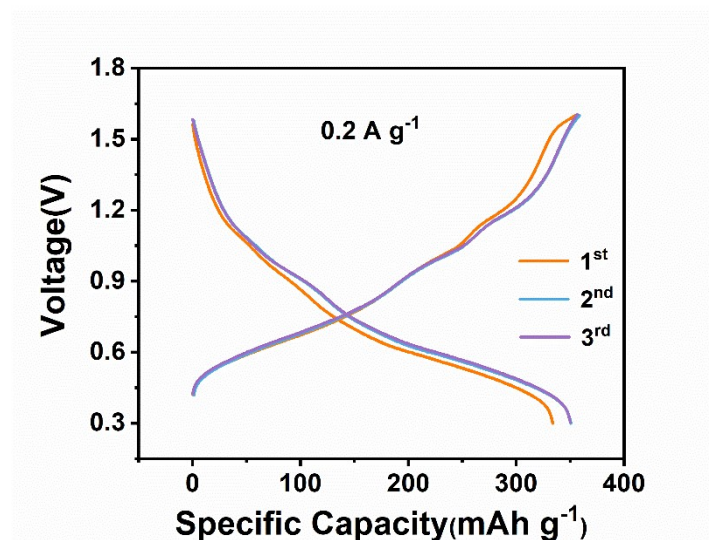


Fig. S10. The GCD curves of $\text{VO}_2@\text{C2}$ at 0.1 A g^{-1} .

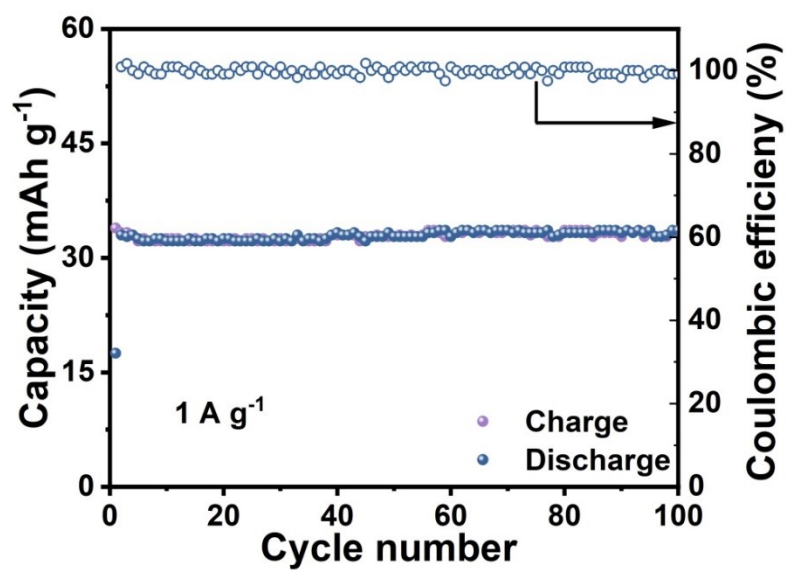


Fig. S11 Cycle performance of carbon substrate at 1 A g^{-1} .

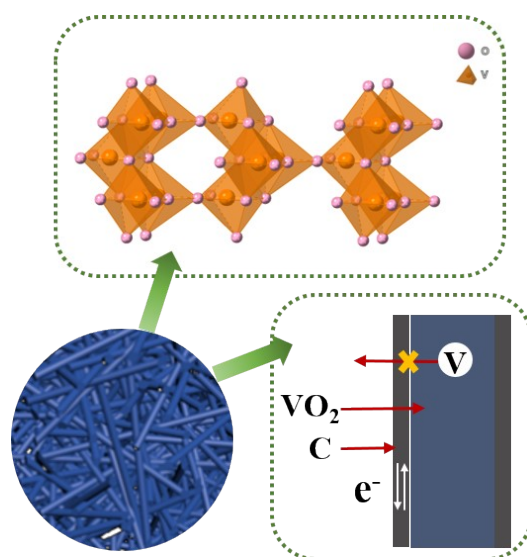


Fig. S12. Schematic diagram of $\text{VO}_2@\text{C}_2$.

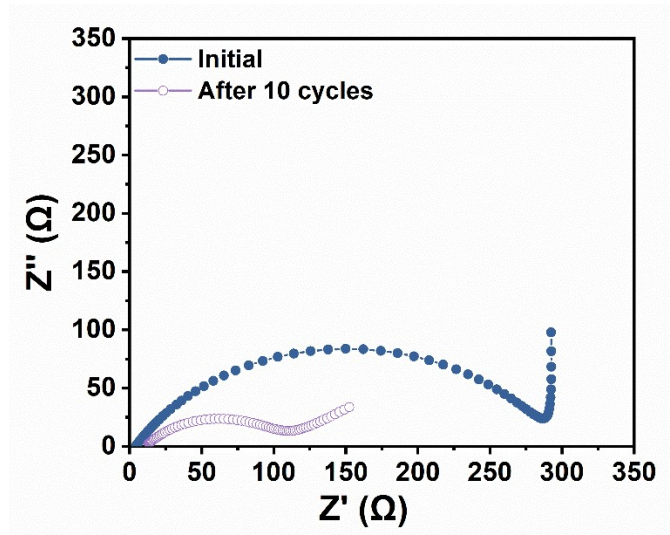


Fig. S13. EIS plots of after 10 cycles

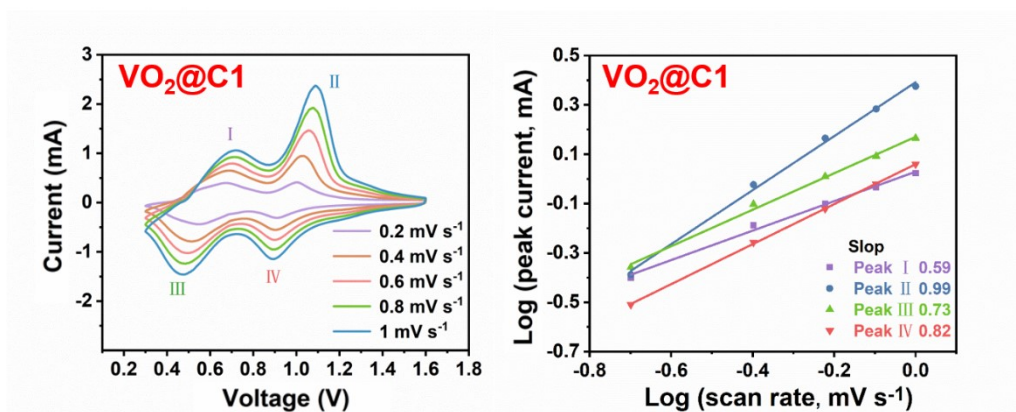


Fig. S14. CV curves at various scan rates of $\text{VO}_2@\text{C1}$ and plots of $\log(\text{peak current})$ vs. $\log(\text{scan rate})$ at each peak from CV curves.

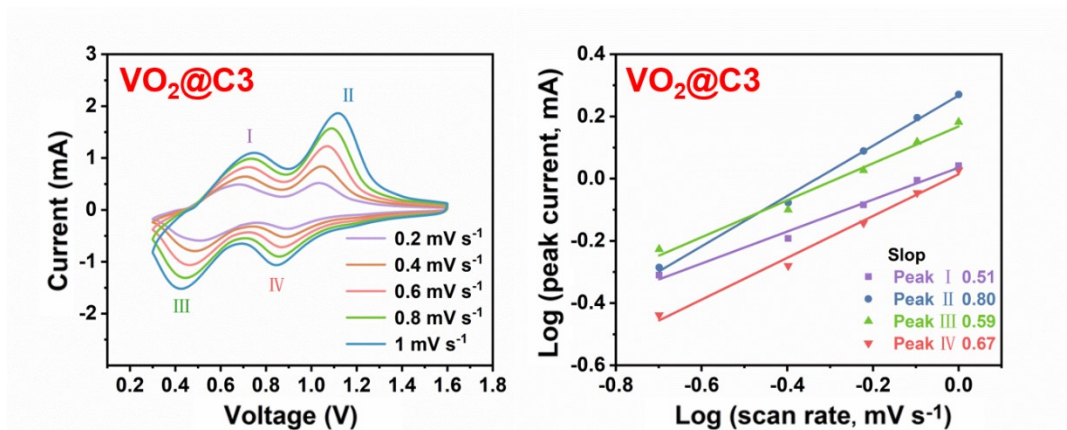


Fig. S15. CV curves at various scan rates of VO₂@C3 and plots of log (peak current) vs. log (scan rate) at each peak from CV curves.

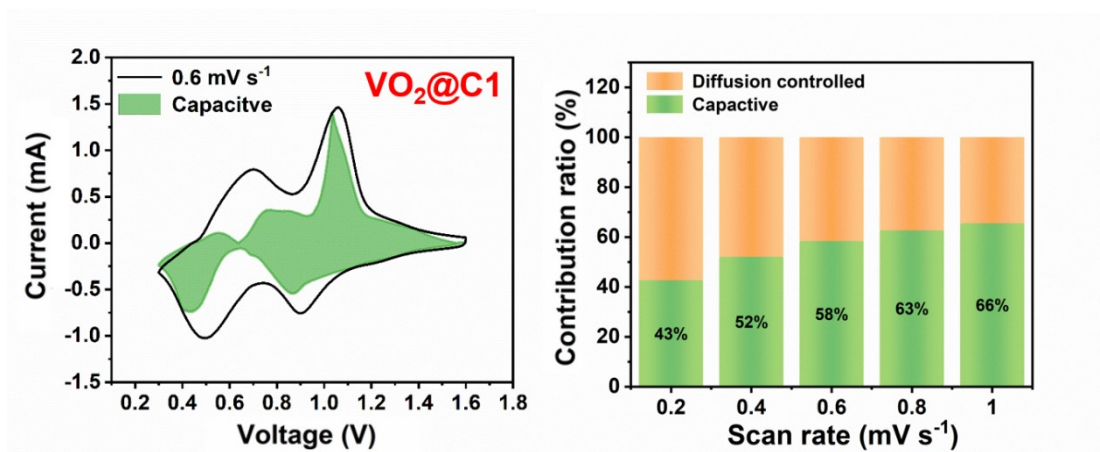


Fig. S16. Capacitive contribution of VO₂@C1 at 0.6 mV s⁻¹. Pseudocapacitive contributions of VO₂@C1 at different scan rates.

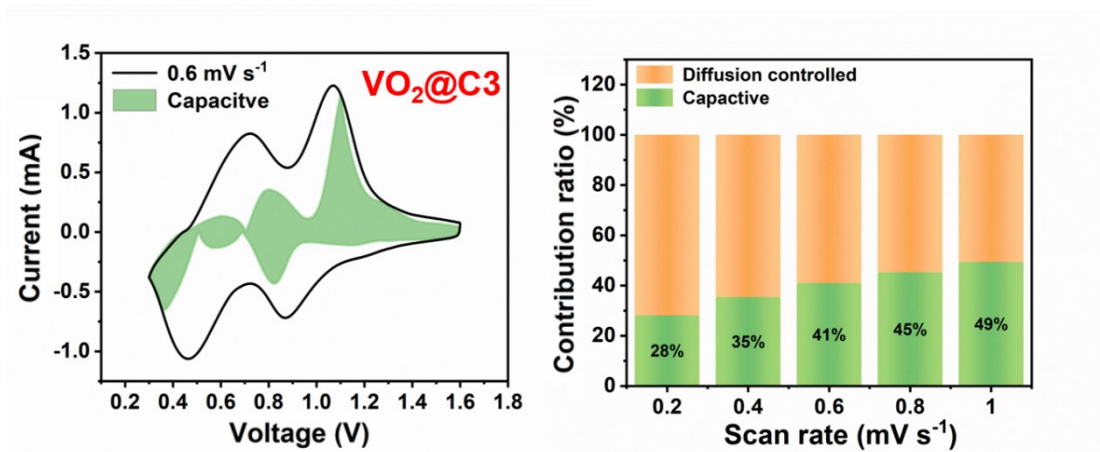


Fig. S17. Capacitive contribution of VO₂@C3 at 0.6 mV s⁻¹. Pseudocapacitive contributions of VO₂@C3 at different scan rates.

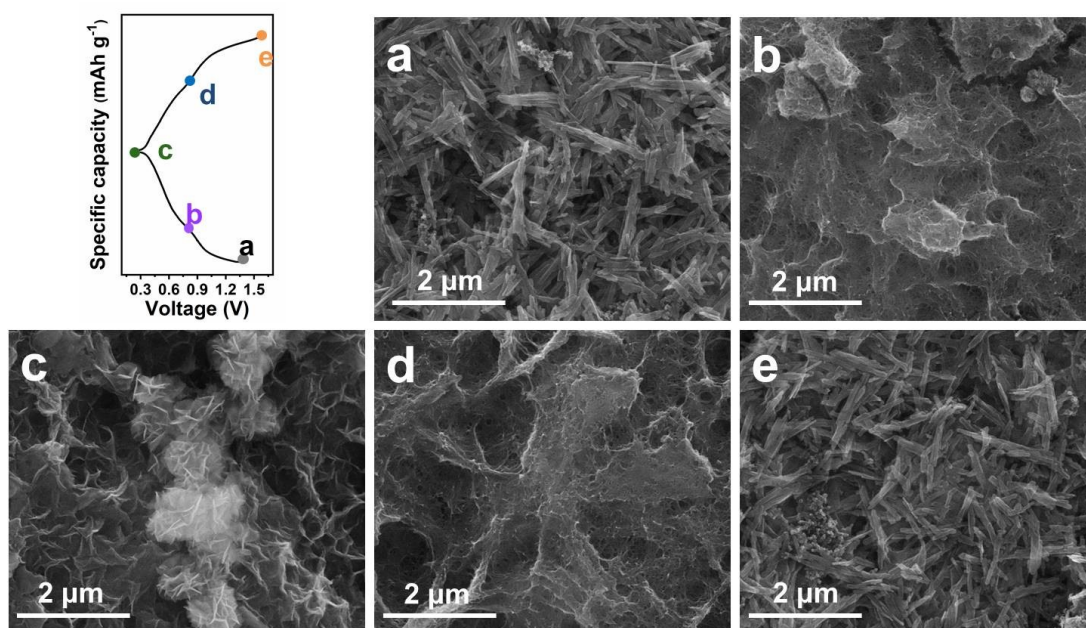


Fig. S18. The ex-situ SEM images of VO₂@C2 composite at different stages.

Note to Fig. S18:

As shown in Fig. S18a, the pristine VO₂@C2 electrode delivers a rod-like morphology. Upon discharge to 0.8 V, the surface of the VO₂@C2 electrode seems to be covered by graphene-like nanosheets (Fig. S18b). According to ex-situ XRD in Fig.

4b, the generation of graphene-like nanosheets are attributed to the phase of $\text{Zn}_{12}(\text{OTf})_9(\text{OH})_{15}\cdot x\text{H}_2\text{O}$, due to the H^+ ions enter into the framework of cathode. Upon further discharge to 0.3 V, the relative diffraction of the $\text{Zn}_3(\text{OH})_2\text{V}_2\text{O}_7\cdot n\text{H}_2\text{O}$ and $\text{Zn}_{12}(\text{OTf})_9(\text{OH})_{15}\cdot x\text{H}_2\text{O}$ phases are observed (Fig. 4b), indicating the amounts of the two new phases are further increased with the deep discharge proceeded, which is due to the insertion of more Zn^{2+} and H^+ ions into the cathode. The graphene-like nanosheets are curled and aggregated into dense nanoflowers, as illustrated by ex-situ SEM images (Fig. S18c). In contrast, upon charge back from 0.3 to 0.8 V, the dense nanoflowers on the electrode become less (Fig. S18d), which originates from the decreased amount of $\text{Zn}_{12}(\text{OTf})_9(\text{OH})_{15}\cdot x\text{H}_2\text{O}$ with the deintercalation of H^+ . When charge to 1.6 V the relative diffraction intensity of the $\text{Zn}_3(\text{OH})_2\text{V}_2\text{O}_7\cdot n\text{H}_2\text{O}$ phase in the ex-situ XRD pattern of the fully charged electrode is much lowered accompanying with the complete disappearance of $\text{Zn}_{12}(\text{OTf})_9(\text{OH})_{15}\cdot x\text{H}_2\text{O}$ (Fig. 4b), indicating the deintercalation of Zn^{2+} and H^+ lead to the recovery of the electrode, which can be further confirmed by ex-situ SEM images (Fig. S18e)..